State of Power Prediction for Lithium-Ion Batteries in Electric Vehicles via Wavelet-Markov Load Analysis

Mona Faraji Niri[1*], Truong Q Dinh[1], Tung Fai Yu[2], James Marco[1], Truong MN Bui[1]

***Abstract*—Electric vehicle (EV) power demands come from its acceleration/braking as well as consumptions of the components. The power delivered to meet any demand is limited to the available power of the battery. This makes the battery state of available power (SoAP) a critical variable for battery management purposes. This paper presents a novel approach for long-term SoAP prediction by supervising the working conditions for prediction of future load. Firstly, a battery equivalent circuit model (ECM) coupled with a thermal model is established to accurately capture the battery dynamics. The battery model is then connected to an EV model in order to interpret the working conditions to battery power demand. By supervising the historical usage conditions, a long-term load prediction mechanism is designed based on wavelet analysis and Markov models. This facilitates the separation of low and high frequency load demands and addresses future uncertainties. Finally, the SoAP prediction is put forward along with a sensitivity analysis with respect to battery model and load prediction mechanism parameters. It is demonstrated that compared to the existing approaches for load and SoAP prediction, the developed method is more practical and accurate. Co-simulations via MATLAB and AMESim as well as experiments on a set of commercially available Lithium-ion (Li-ion) cylindrical cells under real-world drive cycles prove the given concept and validate the performance of the method.**

***Index Terms*— Lithium-ion battery, Load prediction, Markov models, State of power, Vehicle powertrain, Wavelet analysis.**

I. Introduction

GROWING concerns regarding fossil fuel shortage and environment issues has made partial or full electric vehicles increasingly popular because of the opportunities they provide for more secure and less emissions. Li-ion batteries offer several advantages such as high volumetric energy and power density, high cycle lifetime, fast charging, and low self-discharge rate which make them a more promising power source for automotive applications [1, 2]

Battery cells connect in series and parallel to form a battery pack for fulfilling the specific power and energy demand of the vehicle for its acceleration, regenerative braking, gradeability and the energy consumption of ancillary components such as lighting and air conditioning systems. The performance and safety of the battery pack is monitored and controlled via a battery management system (BMS) provided with a set of state measurements and estimations [3]. SoAP is one of the battery states defined as its available charging/discharging power capability [4, 5]. While the power is easily calculated via the multiplication of the measured battery current and voltage, the prediction of SoAP is challenging as it depends on both battery future consumption as well as its dynamics and constraints. SoAP prediction is significant not only for optimizing EV performance and minimizing its energy consumption, but also for moving from a reactive BMS towards a predictive, active or even proactive one for improving the battery performance and protecting it from damage due to overcharge/over-discharge.

Maximum available power (*MAP*) of a battery is derived by the relationship between battery open circuit voltage (OCV) U_{oc}, minimum pack terminal voltage (U_{Tlim}) and its internal ohmic resistance (R_o) [6]:

$$MAP_t = (U_{T_{\lim}} (U_{OC} - U_{T_{\lim}}) / R_o).n_s.n_p \quad (1)$$

where n_p and n_s are the number of cells in series and parallel. This calculation although simple and accurate for laboratory conditions, it is very conservative and not applicable for real world EVs due to the changing impedance of the battery in various driving and ambient conditions (leading to strong time-variability and nonlinear behaviour of the battery). Compared to the considerable number of researchers that have addressed the challenge of battery state of charge (SoC) or state of health (SoH) estimation, the battery power estimation has not been discussed comprehensively. The approaches for power prediction can be divided into two general categories [6]: 1) characteristic maps and 2) model-based methods. Characteristic maps provide information regarding the static interdependency between available power of the battery and a set of internal or external factors such as battery SoC, SoH, temperature, voltage and current [7]. The most common map is developed by the HPPC (hybrid pulse power characterization) test [8] for determining the peak power in laboratory conditions. Characteristic maps, although simple to implement, require numerous experiments to cover all possible scenarios for battery usage in an EV. Considering the stochastic and diverse

The research was undertaken in collaboration with the WMG Centre High Value Manufacturing Catapult (funded by Innovate UK) in collaboration with Jaguar Land Rover Limited. (*Corresponding author, email: mona.faraji-niri@warwick.ac.uk).

M Faraji Niri, TQ Dinh, J Marco and TMN Bui are with Warwick Manufacturing Group, University of Warwick, Coventry, CV47AL, United Kingdom, (e-mail: mona.faraji-niri@warwick.ac.uk, t.dinh@warwick.ac.uk, truong.bui@warwick.ac.uk, james.marco@warwick.ac.uk).

T Fai Yu is with Advanced Battery Engineering, Jaguar Land Rover Ltd, Coventry, CV34LF, United Kingdom, (e-mail: ty5@jaguarlandrover.com).

Color versions of one or more of the figures in this paper are available online at http://ieeexplore.ieee.org.

Digital Object Identifier:

loading conditions in EVs, the SoAP estimated by characteristic maps are generally over optimistic and only valid at the limited range covered by the experimental scenarios designed for generating those maps. Mapping methods normally neglect design limits such as cell current, voltage or power [9] which make them unable to predict the power for the next time step. Improved methods considering battery limitations [10] as well as adaptive methods to regenerate the characteristic maps when the accuracy of the predicted power falls below a threshold are proposed to extend the maps validity range [11]. However, the large memory capacity required for storing multidimensional data of these maps is the main disadvantage for BMS applications [6].

In model-based approaches, a battery dynamical model is employed for online estimation of its states and the prediction of SoAP. Model-based methods face three critical challenges: (1) obtaining an accurate set of battery model parameters and states for variable operating and ambient conditions, (2) the prediction of the future loading conditions, and (3) the design of a computationally efficient and accurate power prediction algorithm. Methods and approaches for battery parameter identification and its state estimation are widely discussed in the literature. Battery parameters are either obtained via offline experiments and stored in the form of lookup tables in the BMS or obtained in an online manner via regression methods [12], least squares-based approaches [13], or adaptive optimization techniques [14]. Battery states such as SoC, internal voltages and SoH are also often estimated by Kalman filters for dealing with noisy input and outputs [5], particle filters for modelling uncertainties [15], observers based on sliding surfaces for addressing nonlinearity in battery characteristics [16], machine learning [17], fuzzy logic [18] and neural networks [19] for cases with less in-depth understanding of battery behaviour. Joint estimation of SoC and peak power is addressed by extended Kalman filters in [20] and [21] by considering voltage limitation, and in [13] by both voltage and current limitations. A comprehensive review on the SoAP prediction methods is given in [6] which confirms that most of the previous studies assume that the battery working conditions remain constant during the prediction interval. It means that the states remain unchanged for the whole prediction horizon which is not true for dynamic operation conditions of EVs.

Available power calculations are normally performed in a prediction horizon of between 1 to 20 seconds [22], at this range the battery SoC, SoH and temperature does not change significantly. But the current and voltage may vary drastically and those are the major limiting factors of power [23]. Battery current and voltage change due to the stochastic loading conditions; this variation if not taken into account will impose an error in the SoAP. The impact of the future load variations on the accuracy of SoAP is overlooked in most of the previous studies by assuming that the future conditions are *a priori* and already known, however the battery future usage depends on so many factors such as road slope, driver behaviour, ambient temperature and traffic flow [24]. Accurate prediction of future loading conditions is therefore necessary for SoAP prediction. There exists different load prediction approaches for batteries in the literature. Methods based on moving average of the historical data [25], wavelet analysis [26], Markov models [27, 28, 29] and neural networks [5, 30] are examples for characterising the future load. However only in a subset of researches [5, 26], these methods have been accompanied with a power prediction mechanism to evaluate their performance.

Considering the abovementioned points, this paper aims to propose a novel approach for long-term prediction of SoAP. It particularly focuses on removing the assumption of *a priori* available load and quantifying the load prediction error effect on the accuracy of predicted battery states. For this purpose, a load prediction model is developed as the new combination of wavelet transformation and Markov models to accurately estimate the future battery load conditions. Both the wavelet and Markov techniques have been recently applied to intelligent transportation systems for traffic condition prediction [31, 32] but not directly connected to battery performance.

The battery load includes components of low frequency relevant to the general consumption of the vehicle, as well as components of high frequency related to the stochastically varying ambient conditions, such as road grade, driver behaviour and parasitic loads. Due to the complex interconnection of above factors, the prediction of load is a difficult task. In this paper, it is shown that the decomposition of frequency domain load data via wavelet technique helps to perform a more in-depth analysis of rapid and slow varying components of load. It is also demonstrated that passing refined load data through the powerful Markov model generates a whole new time series which is very desirable for battery state estimation and prediction purposes such as its SoAP prediction. This study separately quantifies the effect of the future load prediction error on the SoAP as well as the impact of error coming from the battery model parameters or its estimated states on the final predicted power. This will ultimately show that even though an accurate battery model is implemented for SoAP applications, an inappropriate method for future condition prediction will result in poor predictions.

It is worth mentioning that the present study is an extension of the authors' previous research on the prediction of battery end of discharge time [27] based on Markov models. Improving battery electrical-thermal model for accurate representations in different working points, connecting battery model to vehicle powertrain model, designing a wavelet-Gaussian based model parameterisation method for load prediction and experimental validation tests under realistic scenarios are the main contributions of this research compared to the previous one.

The method proposed in this study is evaluated via a co-simulation between AMESim and MATLAB/Simulink. The co-simulation helps to integrate the load prediction mechanism, the battery model and the EV powertrain within a single environment. Furthermore, experimental validations under different loading and ambient conditions are conducted for Li-ion 5Ah cylindrical cells. Discussions on the method details and comparisons with the existing methods for power prediction [26, 27] are also given.

The outline of this paper is as follows: in Section II, the lumped parameter battery model is described. In Section III the

SoAP prediction problem is formulated. The fundamentals of load prediction algorithm are given in Section IV. Section V includes the simulation, experiments and discussions. Finally there are conclusions at Section VI as well as further mathematical details at Appendix Section.

II. Lumped Parameter Battery Model

Various models are developed based on electrical, thermal, chemical and mechanical specifications of the battery. Battery equivalent circuit model is one promising model for online applications like SoAP prediction [33].

ECM consists of resistive-capacitive (RC) networks and an ohmic resistance for transient and stationary response of the battery to input. Larger number of RC networks make the model more accurate but considering the computational burden on BMS, a second order ECM is preferred here.

The battery ECM is represented by a set equations as (2), where, I is battery load current, C is the standard capacity of the cell, v_{pi} is the battery polarization voltage of branch i, U_T is terminal voltage, R_{pi}, C_{pi} are polarization capacitance and resistance respectively.

$$\begin{aligned} SoC &= SoC_0 - \frac{1}{C(T,I)}\int_{t=0}^{t} I_k \Delta t \\ \begin{bmatrix} \dot{v}_{p1} \\ \dot{v}_{p2} \end{bmatrix} &= \begin{bmatrix} -1/\left(R_{p1}(SoC,T).C_{p1}(SoC,T)\right)v_{p1} \\ 1/\left(R_{p2}(SoC,T).C_{p2}(SoC,T)\right)v_{p2} \end{bmatrix} + \\ &\quad \begin{bmatrix} 1/\left(C_{p1}(SoC,T)\right) \\ 1/\left(C_{p2}(SoC,T)\right) \end{bmatrix} I \\ U_T &= U_{OC}(SoC,T) - \sum_{i=1}^{2} v_{pi} - R_0(SoC,T)I \end{aligned} \tag{2}$$

All of the ECM parameters are functions of battery SoC and temperature. Considering that SoAP is estimated in a single cycle of the battery charge/discharge, the battery ageing effect is negligible since the battery capacity does not change significantly in one cycle.

To capture the thermal behaviour of the battery and predict its heat generation and temperature, a thermal model developed

Nomenclature

Acronyms

BMS	Battery management system
DWT	Discrete wavelet transform
EV	Electric vehicle
ECM	Equivalent circuit model
EoD	End of discharge
GM	Gaussian Mixture
HPPC	Hybrid pulse power characterization
MAP	Maximum available power
NEDC	New European driving cycle
PDE	Partial differential equation
PDF	Probability density function
RMSE	Root mean square error
SoC	State of charge
SoH	State of health
SoAP	State of available power
TP	Transition probability
WMM	Wavelet –Markov model

Symbols

a	Approximation signal
α	Road slope [%]
Av	Vehicle frontal area [m^2]
β	Thermal Diffusivity
c_p	Specific heat capacity [$kJkg^{-1}K^{-1}$]
C	Capacity [Ah]
C_A	Air penetration coefficient
CP	Constraint SoAP
C_p	Polarization capacitances [F]
C_m	Cluster index
d	Details signal
δ	Inertia coefficient
η_f	Mechanical transmission efficiency
η_m	Electrical transmission efficiency
φ	Original wavelet function
g	Acceleration gravity [ms^{-2}]
$\bar{\gamma}$	Average temperature gradient [^oC]
h	Convection coefficient [$Wm^{-2}K^{-1}$]
I	Load current [A]
I_M	Identity matrix of order M
k_t	Thermal conductivity [$Wm^{-1}K^{-1}$]

Symbols

l	Wavelet resolution parameter (levels)
λ	Transition probability
Λ	Transition probability matrix
M	Number of clusters
M_c	Battery cell mass [Kg]
M_v	Vehicle mass [kg]
μ_m	Cluster mean
μ	Road and tire resistance coefficient
N	Gaussian PDF
n_s	Number of cells in series
n_p	Number of cells in parallel
Ω	Ohm
p	Probability
PH	Prediction horizon [s]
P_d	Total power demand [W]
P_m	Vehicle power [W]
P_p	Peripherals power [W]
Q	Heat generation [W]
R	Cell radius [m]
r	Radial direction
R_p	Polarization resistances [Ω]
R_0	Ohmic resistance [Ω]
ρ	Cell density [kgm^{-3}]
ρ_A	Air density [kgm^{-3}]
s	Wavelet shift parameter
S	Markov state
δ_m	Cluster variance
Ψ	Basis wavelet function
Δt	Time sample
T_∞	Ambient temperature [^oC]
T	Time series length
T_k	Cell temperature [^oC]
$\bar{T}$	Average temperature [^oC]
U_{oc}	Open circuit voltage [V]
U_T	Terminal Voltage [V]
U_{Tlim}	Minimum pack terminal voltage [V]
v	Vehicle velocity [ms^{-1}]
V_b	Cell buk volume [m^3]
v_p	Polarization voltage [V]
V_T	Terminal voltage [V]
V_{oc}	Open circuit voltage [V]
w_m	Cluster weight
x	Time series
$\mathbb{Z}$	Integer numbers

by [34] is utilised. The model (3) considers a uniform, radially distributed heat with convective heat transfer boundary conditions for r-dimensional temperature distribution of $T(r)$.

$$\rho c_p \frac{\partial T(r)}{\partial t} = \frac{Q}{V_b} + k_t \frac{\partial^2 T(r)}{\partial r^2} + \frac{k_t}{r}\frac{\partial T(r)}{\partial r}$$
$$\frac{\partial T(r)}{\partial r}|_{r=0} = 0, \quad \frac{\partial T(r)}{\partial r}|_{r=R} = -\frac{h}{k_t}(T(R) - T_\infty) \tag{3}$$

where ρ, c_p, k_t and h are volume averaged cell density, specific heat coefficient, thermal conductivity and convection coefficient. R, V_b and T_∞ are the cell radius, bulk volume and the ambient temperature.

The boundary conditions of (3) are obtained via the Newton's law of cooling at cell boundaries. In (3), Q is the heat generation rate of the battery given by (4). The model only considers irreversible heat generation mechanisms and assumes a negligible heat generation due to reversible mechanisms, entropy of mixing, phase and heat capacity change [35].

$$Q = I(U_{oc} - U_T) \tag{4}$$

Equation (3) is a partial differential equation (PDE) and faces computational complexity in on-board calculations. To reduce the calculation cost, a 4th order polynomial is used to approximate the PDE solution [36]. Considering the polynomial approximation along the r-direction as well as the volume-averaged temperature, $\overline{T}$ and temperature gradient $\overline{\gamma}$ as (5) [34], the final two state temperature model is obtained by equations of (6) with $\beta = k_t/\rho c_p$ called the thermal diffusivity.

$$\overline{T} = \frac{2}{R^2}\int_0^R rT(r)dr \ , \quad \overline{\gamma} = \frac{2}{R^2}\int_0^R r\frac{\partial T(r)}{\partial r}dr \tag{5}$$

$$\begin{bmatrix} \dot{\overline{T}} \\ \dot{\overline{\gamma}} \end{bmatrix} = \begin{bmatrix} \frac{-48\beta h}{R(24k_t + Rh)} & \frac{-15\beta h}{24k_t + Rh} \\ \frac{-320\beta h}{R^2(24k_t + Rh)} & \frac{-120\beta(4k_t + Rh)}{R^2(24k_t + Rh)} \end{bmatrix} \begin{bmatrix} \overline{T} \\ \overline{\gamma} \end{bmatrix} + \begin{bmatrix} \frac{\beta}{k_t V_b} & \frac{48\beta h}{R(24k_t + Rh)} \\ 0 & \frac{-320\beta h}{R^2(24k_t + Rh)} \end{bmatrix} \begin{bmatrix} Q \\ T_\infty \end{bmatrix}$$
$$[T] = \begin{bmatrix} \frac{24k_t}{24k_t + Rh} & \frac{15Rk_t}{48k_t + 2Rh} \end{bmatrix} \begin{bmatrix} \overline{T} \\ \overline{\gamma} \end{bmatrix} + \begin{bmatrix} 0 & \frac{Rh}{24k_t + Rh} \end{bmatrix} \begin{bmatrix} Q \\ T_\infty \end{bmatrix} \tag{6}$$

Accordingly, the final lumped parameter electro-thermal model of the battery is obtained in the form of state space equations as a combination of (2) and (6).

III. Long-term SoAP Prediction

The power demand of the battery in EV is directly dependent to its load and varies with vehicle velocity, acceleration, the driver behavior, the road conditions as well as road grade. The power demand of a battery cell in a vehicle with n_s and n_p batteries in series and parallel is obtained via (7), where P_d, P_p and P_m are the total, peripherals and vehicle power demand respectively. η_f and η_m are the mechanical and electrical transmission efficiencies. The function sgn specifies the sign of the vehicle power; positive sign means a power demand while negative means that there is regenerated power due to the recovery effect of the battery or braking events. Here, without loss of generality, it is assumed that the peripherals power demand is zero and vehicle mechanical power follows (8).

$$P_d = \frac{1}{n_s}\left(P_p + \begin{pmatrix} (\eta_f\eta_m)^{-1}(1+\mathrm{sgn}(P_m)/2) + \\ (\eta_f\eta_m)(1-\mathrm{sgn}(P_m)/2) \end{pmatrix} P_m\right) \tag{7}$$

$$P_m = \mu M_v g v\cos\alpha + M_v g v\sin\alpha + \frac{1}{2}\rho_A C_A A_v v^3 + \delta M_v \dot{v} v \tag{8}$$

where M_v is the vehicle mass, A_v is the vehicle frontal area for aerodynamically drag, μ is the resistance coefficient between road and the tires, g is the acceleration gravity, ρ_A is the air density, δ is the inertia coefficient, α is the road slope and C_A is the air penetration coefficient.

From (8) it is obvious that the future demand is related to the future velocity which is interpreted as the load current, I_k, for the battery through vehicle powertrain and battery model. Although the future conditions are unknown at the present time point but they fairly depend on the historical conditions and can be predicted effectively.

Taking I_k as the battery current at time sample k, I_{k+j} determines the current at j time samples ahead. While I_k is measured via current sensors at k, I_{k+j} should be predicated. Considering equation (9), the battery j step ahead voltage is required for power prediction, where PH is prediction horizon.

$$P_{d,k+j} = U_{T,k+j} I_{k+j} \quad j = 1, 2, \ldots PH \tag{9}$$

As the future battery voltage is not readily available, the accurate electro-thermal model for yielding the battery states is necessary.

$$\overline{T}_{k+j} = \left(1 + \frac{-48\beta h\Delta t}{R(24k_t + Rh)}\right)\overline{T}_{k+j-1} - \frac{15\beta h\Delta t}{24k_t + Rh}\overline{\gamma}_{k+j-1} + \frac{\beta\Delta t}{k_t V_b}Q_{k+j} + \frac{48\beta h\Delta t}{R(24k_t + Rh)}T_{\infty k+j}$$
$$\overline{\gamma}_{k+j} = \frac{-320\beta h\Delta t}{R^2(24k_t + Rh)}\overline{T}_{k+j-1} + \frac{(R^2 - 120\beta\Delta t)(4k_t + Rh)}{R^2(24k_t + Rh)}\overline{\gamma}_{k+j-1} - \frac{320\beta h\Delta t}{R^2(24k_t + Rh)}T_{\infty k+j} \tag{10}$$
$$T_{k+j} = \frac{24k_t}{24k_t + Rh}\overline{T}_{k+j} + \frac{15Rk_t}{48k_t + 2Rh}\overline{\gamma}_{k+j} + \frac{Rh}{24k_t + Rh}T_{\infty k+j}$$

According to (2), the battery terminal voltage depends on its

OCV and a set of parameters (R_o, R_{pi}, C_{pi}) varying with temperature and SoC. Therefore, first the future values of temperature and SoC need to be determined. With discrete form of equations given in (6) obtained by Euler's approximation (with the discretization step of 1Hz), the battery temperature will be calculated at j steps ahead by (10).
Via the future current value, the SoC will be calculated by:

$$SoC_{k+j} = SoC_{k+j-1} - \Delta t I_{k+j-1} \big/ C(T_{k+j}, I_{k+j}) \tag{11}$$

SoC_{k+j} along with the future value of temperature will update the parameter set at ECM and deliver the j step ahead battery voltage up to PH as the prediction horizon by (12).

$$\begin{aligned} &\tau_{i,k+j} = R_{pi}(SoC_{k+j}, T_{k+j}).C_{pi}(SoC_{k+j}, T_{k+j}) \\ &v_{pi,k+j} = e^{\frac{\Delta t}{\tau_{i,k+j-1}}} v_{pi,k+j-1} + \\ &\left(1 - e^{\frac{\Delta t}{\tau_{i,k+j-1}}}\right) I_{k+j-1} R_{pi}(SoC_{k+j-1}, T_{k+j-1}) \\ &U_{T,k+j} = U_{OC}(SoC_{k+j}, T_{k+j}) - \sum_{i=1}^{2} v_{pi,k+j} \\ &- R_0(SoC_{k+j}, T_{k+j}) I_{k+j}, \quad i = 1,2 \quad j = 1,2,...PH \end{aligned} \tag{12}$$

It is worth mentioning that although the battery capacity does not change by aging in a single cycle, but it still varies with temperature and current rate (C-rate) of charge/discharge which is considered in (12).

As the battery states vary drastically with the load, online update of its states and parameters provides more accurate results for SoAP compared to the traditional prediction approaches which assume unchanged battery input, states and parameters in the whole prediction horizon.

For guaranteeing a safe and efficient operation of EV, as well as a long lifetime of the battery, the voltage and current of the battery are constrained. This limits the available power of the battery to the constraint SoAP CP_1 under current limits and CP_2 under voltage limits.

$$CP_1 : SoAP_{k+j} = U_{T,k+j|I_{k+j}=I_{\max}} I_{\max}, \; j = 1,2,...,PH \tag{13}$$

$$CP_2 : SoAP_{k+j} = U_{T\min} I_{k+j|U_{T,k+j}=U_{T\min}} \quad j = 1,2,...PH \tag{14}$$

The combination of the both constrained SoAP equations, results the final SoAP given by CP_3.

$$\begin{aligned} &CP_3 : SoAP_{k+j} = \min(SoAP_{k+j|CP_1}, SoAP_{k+j|CP_2}) \\ &\qquad j = 1,2,...PH \end{aligned} \tag{15}$$

The battery limits for voltage and current in charge and discharge strongly depend on the battery physical specifications and usually provided by the manufacturer and included in the battery datasheet. Further constraints on battery temperature, connection resistance, insulation resistance can also affect the deliverable power, these factors can help protecting the battery from damage and improve its lifetime and performance. At this stage these constraints are beyond the scopes of the study and will be addressed in future works.

Assuming that the battery cells in an EV battery pack are similar in specifications, the SoAP for the whole battery pack can be obtained by multiplying the SoAP of a single cell to the number of cells in the pack. Obviously further studies regarding the SoAP in case of inconsistencies between the cells are required in future works.

IV. Load Prediction Mechanism

In the previous section it was justified how the SoAP prediction problem relates to the future load prediction problem, in this section the load prediction mechanism is proposed for determining the j step ahead current and ultimately battery terminal voltage as well as its available power. For this purpose, the battery current is viewed as a stochastic time-series with varying specifications in time and a behavior which can be inferred from its own historical data. For the prediction of load time series, first the features and critical information of its historical data are extracted, then those features combined with a prediction model yield extrapolations. Here to extract load specifications a combination of wavelet analysis-clustering and Markov modelling is proposed. By this approach, first the load data is pre-processed by wavelet transformations, then its features are extracted via a clustering method and then it is forecasted by the Markov model.

A. Wavelet analysis

For batteries, the load is a combination of the low frequency data with high correlation to the previous data, and a high frequency data coming from stochastic ambient conditions such as road grade, driver behaviour and parasitic loads with less correlation to the historical data. By wavelet approach the load time-series is decomposed to details and approximation (trend) signals. This helps to process the components of dataset, which have different specifications, distinctively.

Wavelet transform is a multiresolution analysis method for signals. Its discrete version, discrete wavelet transform (DWT), has two consecutive steps of decomposition, (recognising signal details and trend) and synthesis (obtaining the transform coefficients by up sampling and convolution) [37].

DWT is performed via an original (mother) wavelet function of φ, (16)

$$\varphi_{l,s,k} = 2^{-l/2} \varphi(2^{-l} k - s), \;\; k,l,s \in \mathbb{Z} \tag{16}$$

which is an oscillating, well localised function with a finite vanishing moment [38], with l as the resolution (scale), and s as the shift (translation) parameters. The higher the l, the lower the frequency of decomposed signal.

For a given signal of $x(k)$, wavelet functions give wavelet decomposition coefficients as (17) with $<.>$ as the inner product operator.

$$\varphi_{l,s,k} = \left\langle x_k, \varphi_{l,s,k} \right\rangle = \sum_k x_k \varphi_{l,s,k} \tag{17}$$

The original signal reconstructed via inverse transform is then given by

$$x_k = \sum_l \sum_s c_{l,s} \varphi_{l,s,k} \tag{18}$$

which can be represented by (19) with $\Psi_{l,s}$ as the basis (father) wavelet function. Here, $a_{l,k}$ is the approximation coefficient which shows the trend of the signal and is a slowly varying signal while $d_{l,s}$ is the details coefficient representing the high frequency part of data.

$$x_k = \sum_s c_{l,s} \varphi_{l,s,k} + \sum_s \sum_l d_{l,s} \psi_{l,s,k} = a_{l,k} + \sum_l d_{l,k} \tag{19}$$

This equation is consisted of two operations, a down sampling by 2 at each level, and a convolution over the whole time interval [37]. These operations are similar to low and high pass filtering operations and link φ and Ψ to those filters respectively. The details coefficients are calculated via the inner product of the signal and the basis function:

$$d_{l,k} = \left\langle x_k, \psi_{l,s} \right\rangle = \sum_s c_{l,s} \varphi_{l,s,k} \tag{20}$$

For a DWT with l levels, the original signal x_k: $\{k = 1,2,\ldots T_k\}$, will be decomposed to $l + 1$ sets, with 1 approximation set of length $T_k/2^l$ and l sets of details with length as factors of 2.

B. Markov modeling

While the DWT helps to pre-process the load data, a prediction model is required to obtain its future values. In order to achieve reliable results, a variety of methods and models can be utilized. Among those, Markov models are advantageous due to their capability of representing highly transient time series. Markov models are interesting for prediction applications because of their suitability for memoryless data. A set of data is said to be memoryless if the conditional probability of its present value depends on the probability of one step previous value rather than the probability of the other historical values [39].

After applying the DWT to the load signal, the next step is to construct a Markov model taking approximate and details coefficients as training inputs. The Markov model is specified by its states $\{S_k, k \geq 0\}$ taking values in the finite set $\underline{\mathrm{N}} = \{1, 2, ..., N\}$ following the conditional probabilities of (21).

$$\Pr\left\{S_{k+1} = j \mid S_k = i\right\} = \lambda_{ij} \quad i, j \in \underline{\mathrm{N}} \tag{21}$$

where, $\lambda_{ij} \geq 0$ is the transition probability (TP) from mode i at time k to mode j at time $k + 1$. The transition probabilities are either positive or zero following the total probably law; $\sum_{j=1}^{N} \lambda_{ij} = 1$. Markov model is described by its TP matrix (TPM) of (22) that should be obtained via on the data.

$$\mathbf{\Lambda} = \left[\lambda_{ij}\right], \quad i, j \in \underline{\mathrm{N}} \tag{22}$$

Markov model includes finite number of states/modes; although the number of data points as an input to the model are also finite but devoting one state to each data sample will result in a model with high dimension thus extremely complex for online calculations. To address the challenge of defining the Markov model states and encoding the input data into a small set of states, a data clustering mechanism is utilised. In this approach, the approximation and details signals of the DWT are firstly clustered so each cluster represents each Markov state. Here Gaussian mixture (GM) clustering algorithm is preferred as it is one of the most powerful and computationally affordable clustering techniques [40] .

GM clustering utilises a mixture of Gaussian components in order to cluster a dataset. The output of this algorithm is M clusters $\{C_1, C_2, \ldots C_m, C_M\}$ with distribution function (23), with mean μ_m and covariance σ_m.

$$N(x; \mu_m, \sigma_m) = \frac{1}{(2\pi\sigma_m)^{1/2}} \exp\left(-\frac{(x-\mu_m)^T (x-\mu_m)}{2\sigma_m}\right) \tag{23}$$

Based on GM clustering algorithm, the probability density function (PDF) of data follows (24) where $p(x|m)$ is the PDF of cluster C_m with w_m as its associated weight following $\sum_m w_m = 1$.

$$p(x) = \sum_{m=1}^{M} w_m p(x \mid m) = \sum_{m=1}^{M} w_m N(x; \mu_m, \Sigma_m) \tag{24}$$

Here, the parameters of the clusters are obtained via expectation maximization which maximizes the likelihood of a set of parameters belonging to a specific cluster [41].

Clustering the approximation and details coefficients will provides states for the Markov process and based on the cluster index of each sample point, the Markov model is trained (the TPM can be calculated). Considering Markov property of data, the probability of observing the specific state of S_k at the time k is firstly calculated by (25).

$$\Pr(S_k = s_k) = \Pr(S_1 = s_1) \prod_{k=2}^{T} \Pr(S_k = s_k \mid S_{k-1} = s_{k-1}) \tag{25}$$

Starting from an initial condition, the TPM matrix is obtained by optimising the likelihood function of (26) which shows the likelihood of transition from cluster i to j with m_{ij} as the total number of transitions [42].

$$L(\Lambda, S) = \Pr(S_1 = s_1) \prod_{i=1}^{N} \prod_{j=1}^{N} \lambda_{ij}^{m_{ij}} \tag{26}$$

The wavelet-Markov (WMM) model is advantages over the conventional Markov model due to the following three reasons:

1) The battery load shows considerable high frequency variations, and this severe volatility makes it difficult to correctly identify the load trend. DWT will help decomposing the load signal for further analysis.
2) In the latter method, the high and low frequency components of the load are predicated via a single Markov model, although they are affected by totally different

factors, have different sources and change with different patterns. Obviously, separate Markov models for trend and details signals in WMM will perform more efficiently. This method helps to correctly forecast small movements without missing the bigger and more significant ones in load.

3) Via DWT, the trend of the signal is represented with fewer number of data points therefore prediction algorithm needs to process fewer data in each Markov model.

Furthermore the method is advantageous over the popular moving average methods [27] because:

1) Moving average methods are lagged regarding the original load and are unable to identify the new changes in trend and regimes.
2) Moving average methods are similar to low pass filters with the main drawback of hindering the transient and intense movements that may turn to be quite important.

To summarize, the diagram of the proposed algorithm is depicted in Figure 1.

Based on the constructed model, the following steps provide the future load values:

- Prediction of the next load cluster via Markov model
- Generation of approximate and details signals based on the next cluster features following a Gaussian probability density function.
- Reconstruction of the load signal via inverse DWT.

V. Simulations and Experiments

In order to evaluate the proposed load and SoAP prediction algorithm, 5Ah commercial $LiFePO_4$ cells at 100% SoH are utilised. The vehicle battery pack is assumed to be configured of 114 cells in series and 17 strings in parallel. The battery model is implemented in MATLAB and the vehicle powertrain is established in AMESim following co-simulation configuration.

A. Experimental setup

An experimental setup shown at Figure 2 is designed to cycle the battery cells. This setup includes a battery cycler Maccor™ series 4000H, a computer (1.90 GHz, 2.11 GHz CPU,16.0 GB RAM) to control the charge/discharge currents of the battery, the temperature of the thermal chamber, simulations of battery and vehicle model as well as running the programmes and algorithms. It also has a test tray including 4 batteries from the same manufacturer with temperature, current and voltage sensors, and a thermal chamber from Binder™. The sampling time is considered to be 1Hz.

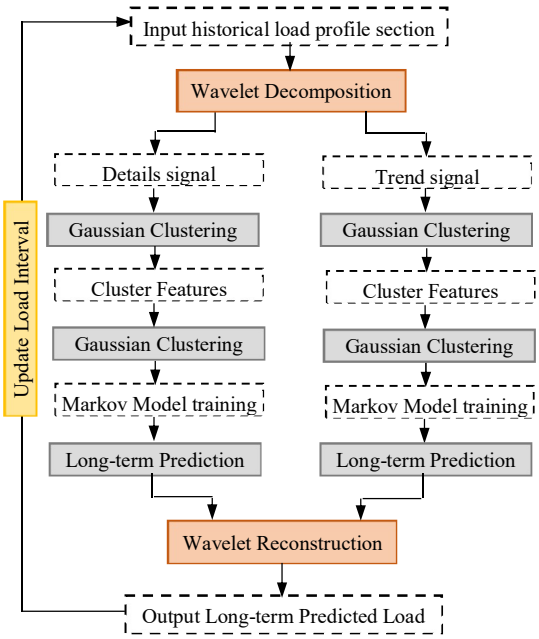

Figure 1.Block diagram of the WMM for load prediction

To reduce the effect of the inconsistency between the individual batteries, the average values of all the cell measured are reported hereafter.

Before running the validations tests, initial tests were conducted to fully characterize the battery. For this purpose, firstly the battery total capacity was estimated via constant current constant-voltage (CC-CV) protocol for charging it up to the cut-off voltage of 4.2V starting from the lower cut off of 2.5V, with the current chosen to be 0.2C, 0.5C, 1C and 1.5C at 4 distinctive temperatures of 5, 10, 25, 40°C and then discharging protocol with constant current of 1C until the cut-off voltage. Each temperature change was followed by a rest time of 4 hours to ensure thermal equilibrium. The maximum

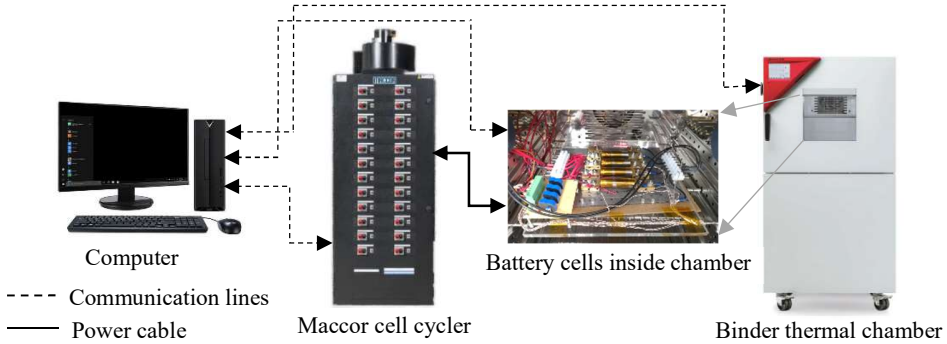

Figure 2. Experimental setup of the research

available capacity of the battery is given at Figure 3.

As Figure 3 shows the capacity of the cell reduces as the discharge C-rate increases, a reduction in capacity is also obvious as the ambient temperature gets lower. The results are compatible with the previous experimental results reported in the literature [43, 44].

According to the datasheet of the cell, cycling the batteries under very low or very high C-rates at some temperatures was not allowed due to safety concerns. So the test results are limited to the ranges recommended by the manufacturer as shown in Figure 3. For capacity estimation, the standard coulomb counting method was utilised.

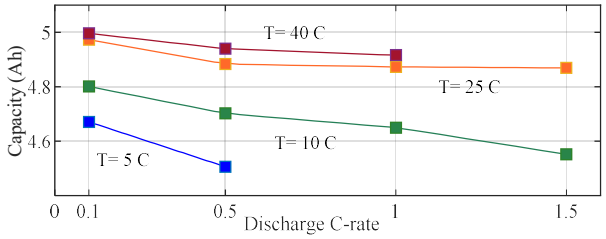

Figure 3.Maximum capacity of cells under different temperature and C-rates

B. *Vehicle Powertrain model*

The powertrain model for EV with customized battery model is given in Figure 4 with vehicle model parameters of Table 1.

Table 1. The EV model parameters

Parameter	η_f	η_m	n_s	n_p	g	A_v
Value	0.98	0.95	114	17	9.8	2
Parameter	C_A	α	μ	δ	ρ_A	M_v
Value	0.3	0	1	0.5	1.22	1360

Assuming that the vehicle acceleration is obtained from its navigations and positioning system the vehicle velocity and road grade are passed through a driver plus EV powertrain model to provide the battery current demand (in Amps).

The motor used for the simulation is a customized one with the default parameter set, specifications and characteristic maps in AMESim toolbox suitable for the electric vehicle technology. The flux linkage-current maps for vehicle its permanent magnet synchronous motor along with *d-q* axis currents are given at Figure 5 assuming symmetry in data. Number of motor poles is 4. It has stator winding resistance of 0.049Ω, stator end winding inductance of 0.149mH, *d* axis stator cyclic inductance of 3.825mH and *q* axis stator cyclic inductance of 14.88mH.

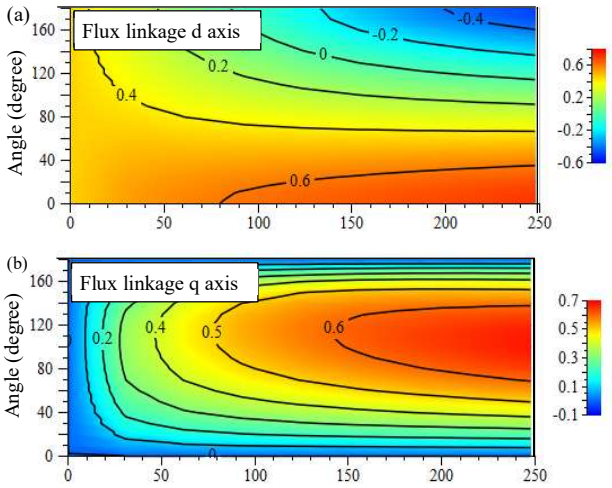

Figure 5. (a) I_d, (b) I_q RMS magnitude (A)

C. *Battery electro-thermal model*

To obtain the parameters of the battery electro-thermal model, a set of standard characterization tests are conducted. For this purpose the pulse power test is designed. In this test a

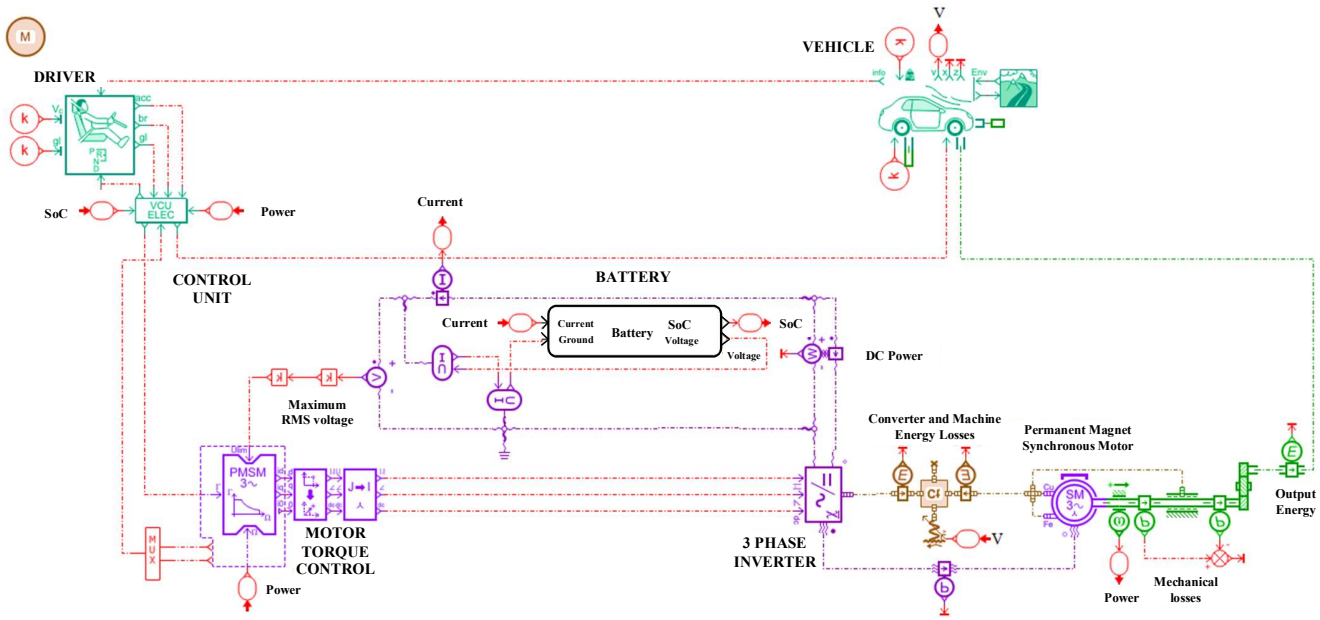

Figure 4. The powertrain model of the EV with customized battery model

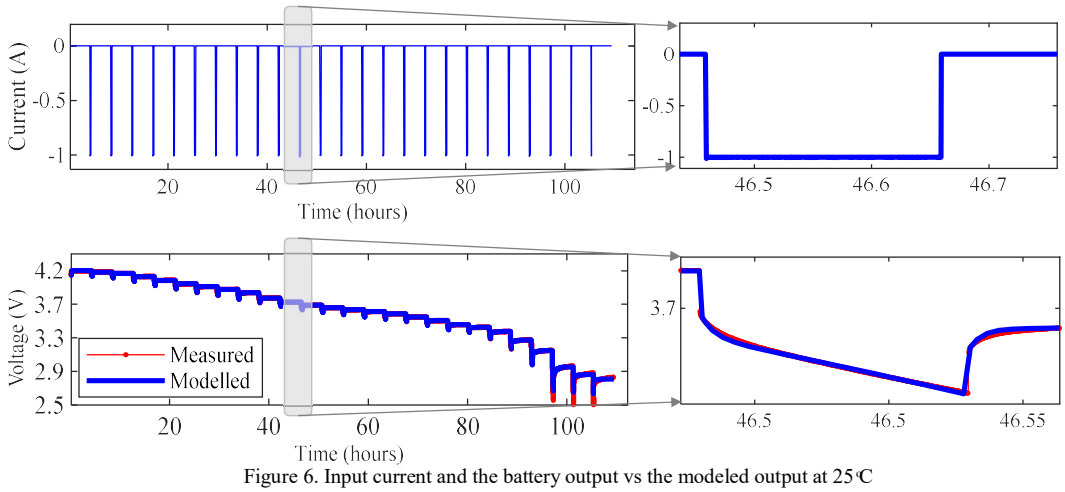

Figure 6. Input current and the battery output vs the modeled output at 25℃

pulse current is applied to the battery which leads to a 4% discharge and follows a 4 hour rest to ensure stable results. The current profile and the battery output voltage under this test are given in Figure 6. The sampling time for modelling is set to 0.01Hz to capture the variations and obtain accurate results.

Via least squares-based optimisation, the parameters of the ECM are obtained at each 4% breakpoint of SoC. The pulse test with the 0.2C rate is repeated at 4 different temperatures of 5, 15, 25 and 40℃ to capture the dependency of the cell model parameters to the ambient and cell temperature. The dependency of full set of battery parameters to SoC and temperature is plotted in Figure 7.

The obtained model shows a root mean square error (RMSE) of 1.85 mV and the maximum error of 221.39 mV at the end of the discharge range when the battery shows more non-linear behaviour. Further details on optimising the battery ECM model is given in [45].

The parameters of the battery thermal model are given in Table 2. The battery dimensions and weight is obtained via its technical datasheet. The *h* value depends on the cooling system efficiency and from optimization techniques is set to 15 for the air forced cooling strategy in a thermal chamber [46]. The battery specific heat coefficient depends on its chemistry.

Table 2.Parameters of the battery thermal model

Parameter	M_c	R	L	h	k_r	C_p
Values	0.068	0.0115	0.070	15	0.25 [47]	1050 [48]

D. Results

In this section the method for SoAP prediction is validated.

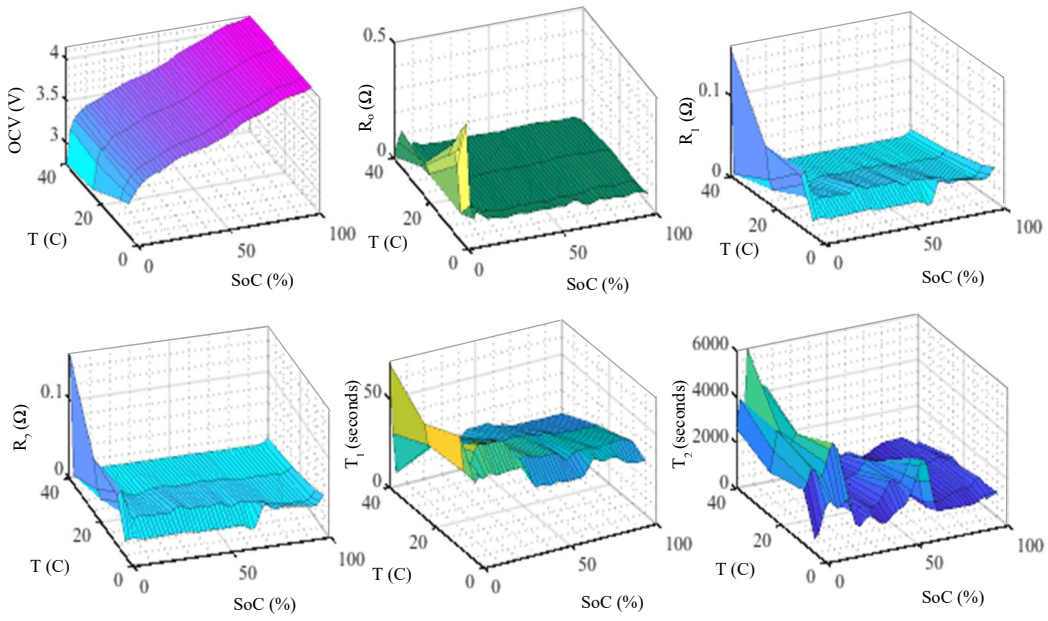

Figure 7. Battery OCV and ECM parameters under different SoC and temperature conditions

For this purpose three loading cases are taken into account. Each case has different load demands and ambient temperature. All the signals are obtained via 5 distinctive Monte-Carlo runs for stochastic algorithms to provide confident results. The predication and measurements are both obtained with 1Hz sampling rate.

For validations, the electric vehicle model was first developed in AMESim with the customised battery model developed in MATLAB based on parameterisation and characterisation tests. The Artemis and NEDC speed profiles were obtained from literature while Coventry profile was directly recorded from real-world motorway driving. The profiles were than applied to the AMESim vehicle model to obtain the battery input current. Those currents were in turn utilised to cycle batteries inside the thermal chamber and connected to the battery cycler as well as a computer.

D.1. Power prediction under Artemis motorway loading at 25°C

The Artemis cycle is a benchmark loading profile representative of average to aggressive driving. The velocity profile of Artemis motorway is depicted in Figure 8. Passing this profile through the vehicle powertrain model and considering the number of cells in series and parallel in the vehicle, the current profile for a single battery is as Figure 9.

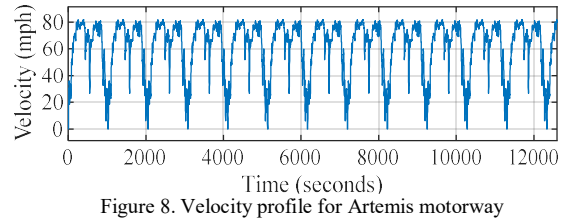

Figure 8. Velocity profile for Artemis motorway

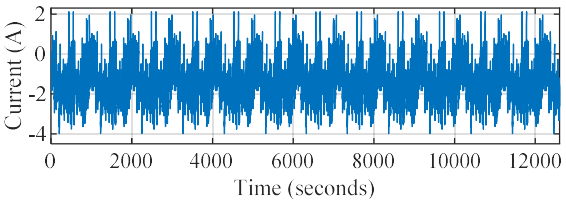

Figure 9. Current profile for Artemis motorway

The battery ECM-thermal model error via the experiments is given in Figure 10. The voltage prediction error is less than 0.05V in the whole discharge range (100 to 5% SoC) and shows a maximum error of 0.1 V at the end of discharge where the battery is more nonlinear. The error of temperature prediction is also less than 0.15 ^{0}C in whole range.

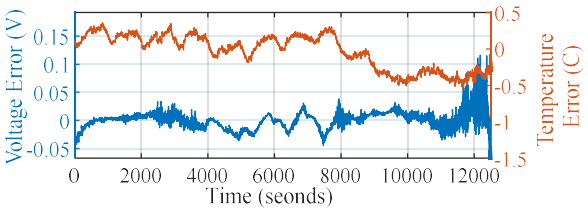

Figure 10. Temperature and voltage modeling error for Artemis profile

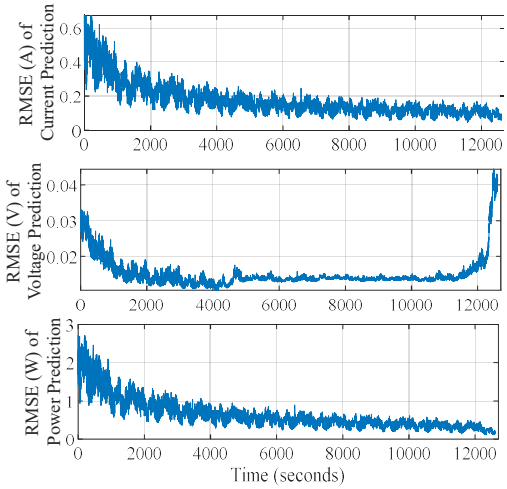

Figure 11. Evolution of prediction RMSE under Artemis profile over time

Figure 11 shows the RMSE of current, voltage and power prediction for the Artemis loading scenario. According to this figure, the error is under 0.6A for current, under 0.03V for voltage and under 3W for power in whole discharge range. The average RMSE for current prediction is 0.16981A, for voltage is 0.015091V and for power prediction is 0.62375W. The values of the error confirm the capability of this method.

Figures 12-14 show the ground-truth battery current, voltage and power versus the predicated ones by the WMM method following (12). The distribution of the historical and predicted current signals are also provided. Figures are snapshots of dynamic sections of the Artemis cycle. The intervals are representative of low, medium and high SoC ranges.

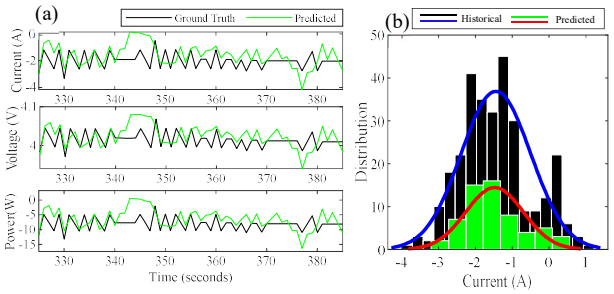

Figure 12. Predicted states (a) and current distribution (b) at low SoC interval of Artemis profile

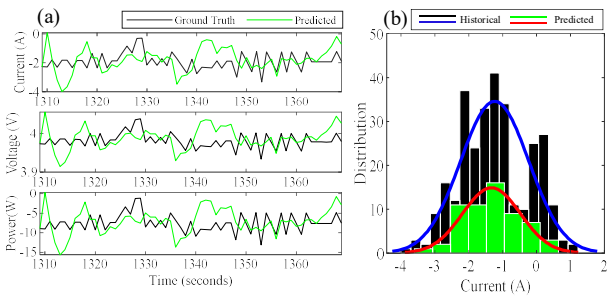

Figure 13. Predicted states (a) and current distribution (b) at medium SoC interval of Artemis profile

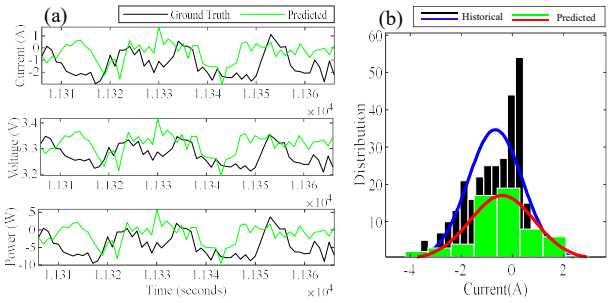

Figure 14. Predicted states (a) and current distribution (b) at high SoC interval of Artemis profile

The difference between predicted and ground truth current is the main source of the error. Rather small terminal voltage prediction error is a result of the battery dynamical behaviour. Battery works as a low-pass filter for the input current and reduces the prediction error for output.

The results show that in spite of deviations between the predicted and the actual values, the general trend of signals is the same and the increase and decrease in signals are well predicted. It is also worth mentioning that, the load prediction method is based on feature extraction of historical data and modelling based on probability theory for the generation of future values. Since this is a stochastic method, the difference between the actual and predicated values were expected. Rather than expecting every the single value in the forecasted load to be exactly similar to the actual load, it is expected that predicted and historical data follow the same probabilistic features, which is confirmed by the distribution charts of each interval in the all previous figures.

D.2. Power prediction for Coventry motorway loading at 10ºC

Figure 15 shows the data of velocity logged from a vehicle within Coventry, UK motorway. The current profile in Figure 16 shows a very high demand and high current charge/discharge profile. The ambient temperature around battery is fixed at 10^0C to examine the accuracy of the method at low temperatures. The initial SoC is set to 100% and cut off SoC is 5%.

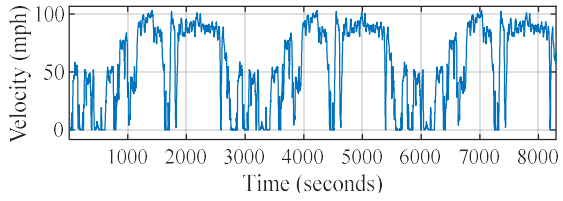

Figure 15. Velocity profile for Coventry motorway

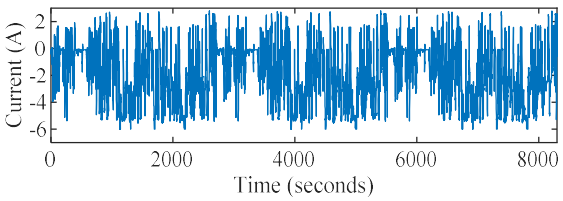

Figure 16. Current profile for Coventry motorway

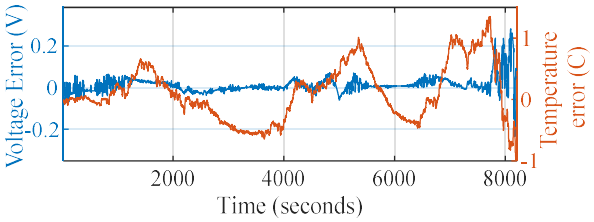

Figure 17. Temperature and voltage modeling error for Coventry profile

For this scenario, Figure 17 shows that modelling error for voltage is in the range of 0.05V and the maximum value of 0.25V at the end of discharge time. The temperature modelling error is limited to 1.1 ^{0}C in whole range.

The RMSE of the predicted states is given in Figure 18.

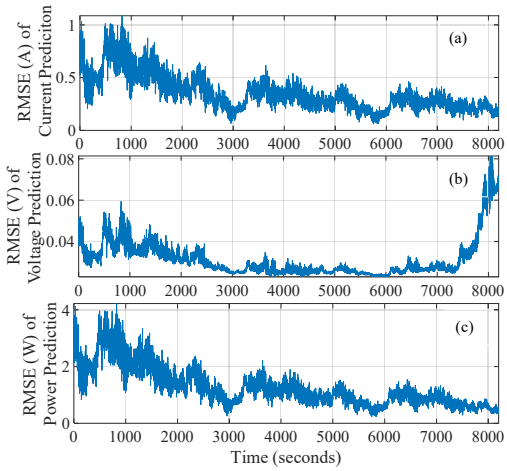

Figure 18. Evolution of prediction RMSE under Coventry profile over time

According to this figures, the RMSE of voltage prediction is highest at the end of discharge time due to model inaccuracies at that interval. The average RMSE for predicted current is 0.350A, for voltage is 0.0313V and for power is 1.260W.

Examples of predicted current, voltage and power signals at different SoC intervals are given in Figures 19-21. Since the predicted current has some difference with the actual current, the predicted voltage and power show some error. However, the general trend and most of the peaks and dips which are related to the acceleration and braking events are captured correctly.

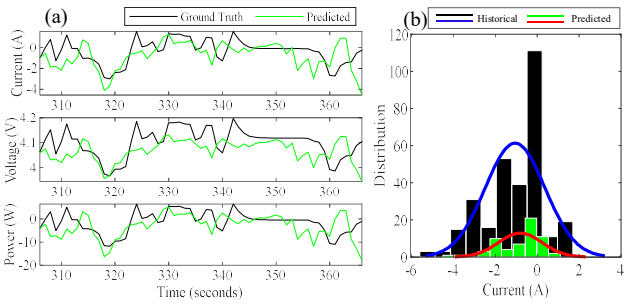

Figure 19. Predicted states (a) and current distribution (b) at low SoC interval of Coventry profile

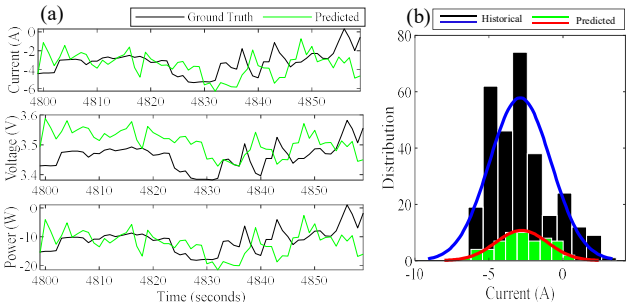

Figure 20. Predicted states (a) and current distribution (b) at medium SoC interval of Coventry profile

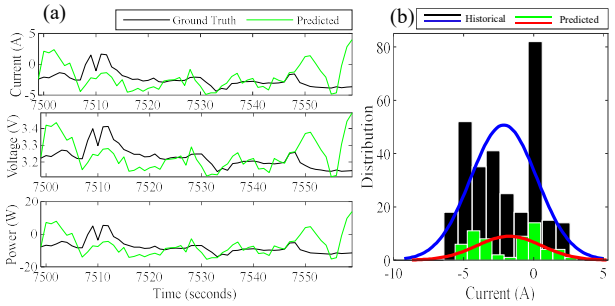

Figure 21. Predicted states (a) and current distribution (b) at high SoC interval of Coventry profile

D.3) Power prediction under NEDC loading at 40°C

New European Driving Cycle (NEDC) is representative of passenger cars in normal European roads with velocity and current profiles given in Figures 22 and 23. For this scenario the battery initial SoC is set to 95% at ambient temperature of 40°*C*. The cut off SoC is 5%.

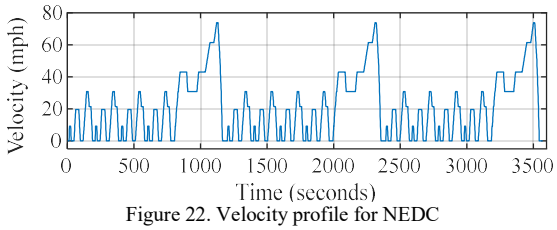

Figure 22. Velocity profile for NEDC

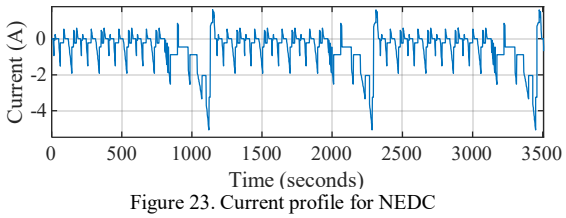

Figure 23. Current profile for NEDC

For the NEDC loading scenario, the average RMSE of predicted current is 0.197A, and the RMSE of predicted voltage is 0.007V and the RMSE of predicted instantaneous power is 0.782W. The time evolution of error is depicted in Figure 24.

The snapshots of the current, voltage and power prediction results are in figures 25-27. They show the performance of the proposed method. The error trend at this profile is also very similar to the previous cases, with the maximum voltage error at the end of discharge time of the battery.

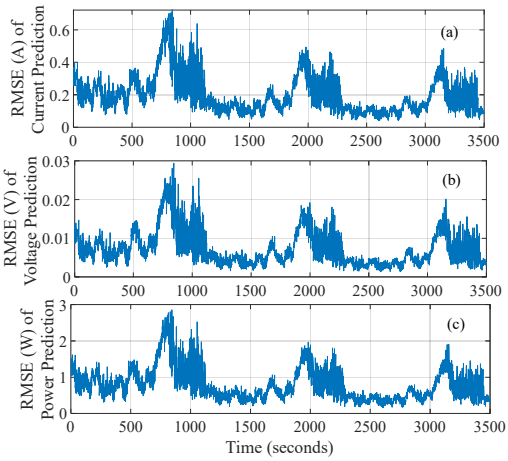

Figure 24. Evolution of prediction RMSE under NEDC profile over time

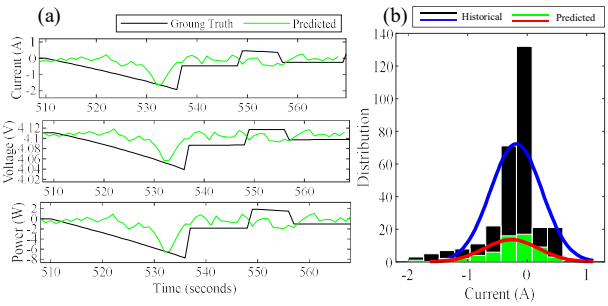

Figure 25. Predicted states (a) and current distribution (b) at low SoC interval of NEDC profile

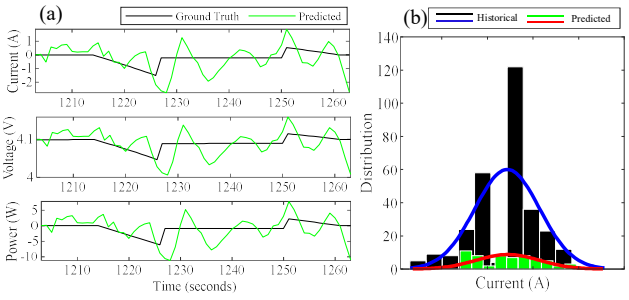

Figure 26. Predicted states (a) and current distribution (b) at medium SoC interval of NEDC profile

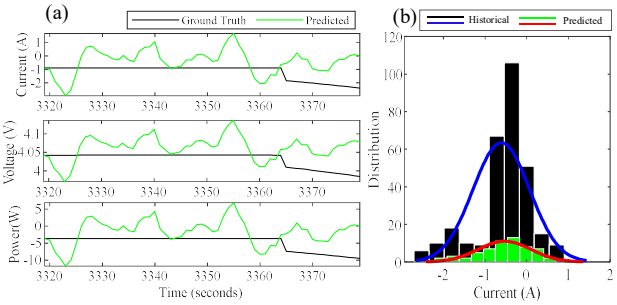

Figure 27. Predicted states (a) and current distribution (b) at high SoC interval of NEDC profile

Comparing the three load profiles and the error in the prediction of battery states, the Figure 28 summarises the error for SoAP following the definition in (15). The RMSE of SoAP prediction always remains below 2W for all cases. By translating the RMSE of the predicted SoAP to the percentage of its average value, which is based on the average load current at the whole discharge range and the battery nominal voltage, 3.63V the SoAP prediction error will be 8.773% for Artemis, 12.35% for Coventry and 23.81% for NEDC.

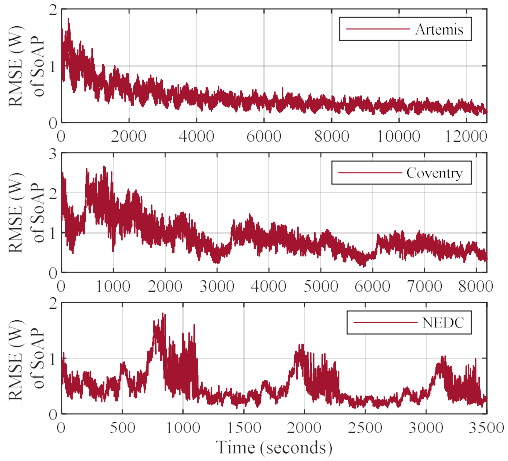

Figure 28. RMSE of SoAP predication for three loading scenarios

E. Discussions

Further discussions about the selection of the Wavelet-Markov prediction method parameters are given in this section.

1) Wavelet functions: There exist a variety of wavelet functions and the type of function depends on the application. Generally the chosen wavelet function should resemble the load shape. However, as the load profiles are very different in different driving styles and ambient conditions, no specific function is preferred over the others. In this study the Symlet wavelet of order 6 [38], Figure 29, is utilized due to is asymmetric shape. Based to the simulations, there is not a significant difference in the final accuracy of predicated results for other functions.

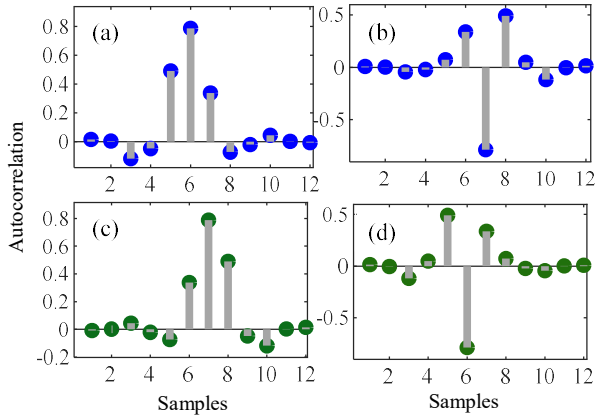

Figure 29. (a) Decomposition low pass filter, (b) Decomposition high pass filter (c) Reconstruction low pass filter, (d) Reconstruction high pass filter of Symlet6.

2) Level of decomposition: Higher levels of decomposition provides smoother approximate signals with fewer number of samples. Also it generates more detailed signals with data more exactly separated based on the frequency. As in this study each of the approximate and details signals connect to a specific Markov model, higher levels will necessitate more Markov models to be trained and implemented. Therefore the selection of this parameter is dependent to the affordable computational burden. In this study the decomposition is assumed to be performed with level 2.

3) Number of clusters: The number of clusters is a critical parameter with direct impact on the computational complexity and the quality of the clustering. Large number of clusters although provides a more specific clusters with high levels of similarity between the data, but may result in overfitting as well as computational complexity. On the other hand, too few clusters may result in a model unable to represent the whole data properly. Discussions on the effect of the cluster number on the quality of clustering procedure can be found in [45]. In current study the number of cluster is set to 2. These 2 clusters will be representative of maximum and minimum values in the load time series.

4) Length of training data: The number of data points used for training the Markov model affect the complexity of the algorithm and its accuracy. While a large data set impose more uncertainty and noise into the model, a small data set may not be able to capture the trend and transitions in the load for forecast purposes. Here, as a compromise between fidelity and complexity, the number of historical data samples is set to 300.

5) Clustering and Markov model initial probabilities: Expectation maximization for both clustering and Markov modeling is an iterative procedure which requires initial conditions. Here, the initial conditions for clustering algorithm are set equally for all clusters as $\mu_{0,m} = avg(x)$, $\sigma_{0,m} = std(x)$, $w_{0,m} = 1/M$ which avg(x) is the mean value, std(x) is the standard deviation of the whole data and the cluster weights are assumed to be equal *[49]*. The initial values of the TPM is assumed to be $\Lambda_0 = 1/M^* I_M$, where I_M is the identity matrix of order M, which presumes an equal probability for transition from each mode to the other at the initial step.

The proposed method provides an accurate long-term prediction for SoAP, however, it is a model-based method and relies on the accuracy of the parameters set obtained for the battery model. Further discussion are given below to clarify the modeling and the proposed prediction algorithm contributions in the performance of the battery.

6) Modeling vs load prediction error: The error in the predicted battery states is originated both from the error in the battery model as well as the error imposed by the load prediction mechanism. Table 3 summarizes the error. According to this table the effect of load prediction error is much more considerable that the effect of battery modelling error. To summarize, between 96-99% of error comes from the

load prediction mechanism while only 4-1% is related to battery modeling error.

Table 3. RMSE of power and voltage prediction vs modelling errors

Method	Case study	Artemis	Coventry	NEDC
Power	Modeling error	0.6237	1.2606	0.7822
	No Modeling error	0.6229	1.2588	0.7811
Voltage	Modeling error	0.0150	0.0313	0.0072
	No Modeling error	0.0070	0.0142	0.0033

7) Non-repetitive loading profile: For the three previously included loading scenarios, the length of the signals were not sufficient to fully discharge the battery, therefore the load profiles were repeated to get enough length of input for complete discharge of the battery. To test the performance of the method on a non-repetitive load profile, a synthetic loading current is utilized. In this case some well-known loading scenarios were combined together to provide enough length as given in the Figure 30. High performance loading [50], Artemis motorway, Artemis urban and Coventry motorway loading are the sections of this loading profile, which are connected together in an arbitrary order. For this case, RMS error is 0.270A for current predication, 0.0119V for voltage prediction, 0.971W for power prediction and 0.6768W for SoAP prediction. According to Figure 31 the method provides desirable results even though the battery has gone under non-repetitive loading profile.

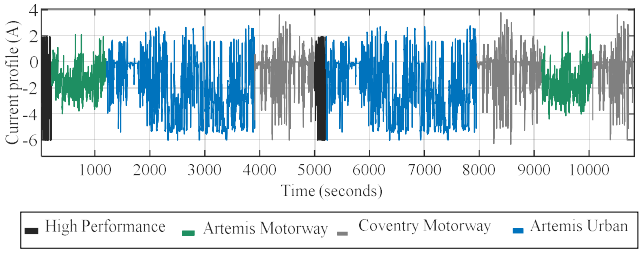

Figure 30. Combined loading profile

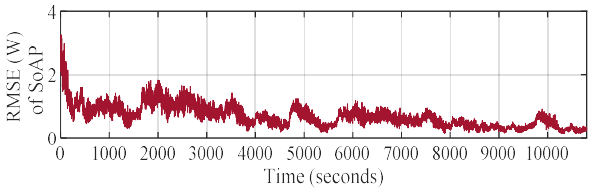

Figure 31. SoAP prediction error for combined load profile

8) Computation time: Simulations showed that an average of 0.6% of each sample time is dedicated to Wavelet-Gaussian-Markov prediction algorithm to generate future load data, and an average of 1.08% is dedicated to run battery thermal and electrical model. There is an average of 88.6% of each sample time remaining for other battery management systems functions. Based on the computational complexity and timing of the method, it is believed that the algorithm is easily implementable in real-time.

9) Comparisons: To analyze the effect of the load prediction mechanism for the SoAP, the proposed method is compared with two similar cases. The first case is where the load is obtained via wavelet analysis proposed in [26], and the second case is where the future conditions are predicated via Markov model [27]. The results are given in Table 4.

Table 4. RMSE analysis for SoAP prediction by different approaches

Method	Artemis	Coventry	NEDC
Wavelet Markov	0.4246	0.8752	0.4873
Wavelet [26]	0.7807	1.4900	0.8070
Markov [27]	0.6272	0.9550	0.4892

The results in the table show that the combination of wavelet-Markov modelling techniques provides the highest accuracy for all load profiles. The improvements for Artemis and Coventry load profiles are more highlighted as those are more transient loading styles which cannot be addressed via only wavelet, or Markov method. Obviously the increased accuracy comes with the increased cost of algorithm design as the proposed method has more design variables than the other ones. A compromise between method tuning efforts and the accuracy is required for final implementations and is a problem to be addressed via optimization techniques in future studies.

VI. Conclusion

Alongside SoC, and SoH, SoAP facilitates a reasonable energy management strategy in EVs. As a prediction problem, it strongly relies on the load prediction mechanism and its accuracy to characterize future conditions. The Markov model although very popular for analyzing time sequences, cannot provide accurate results when applied for highly irregular data. In this study this deficiency is addressed via a Markov model given slowly and rapidly varying components of load data separated via wavelet analysis. The investigations shows that the load prediction error has much more contribution in the final error of predicted power compared to the battery modeling error. This implies that more serious efforts are required for improving vehicle power prediction. Simulations and experimental validations show that the wavelet-Markov method is more promising for very transient load profiles. However there are still a few main areas for extending the current work, i) developing an optimization technique for the selection of the design variables of the method, ii) modifications to the designed strategy to make it more appropriate for more diverse use cases, iii) utilizing multi-physics-based battery models in order to perform SoAP prediction subject to physics based constraints beside current, and voltage limits, iv) developing a more detailed vehicle powertrain model more focused on dynamic behavior, including nonlinear elements such as tyre model and both longitudinal and lateral behaviour, and finally v) fully assess the scalability of this approach when validating its performance at full system level. Final deployment of the methodology within a BMS must take into account additional uncertainties, for example those associated with the heterogeneous behavior of the connected cells and integration of SoAP algorithms with other control functions.

APPENDIX

Derivation of state space thermal equations: The solution of the PDE (3) is approximated by the following polynomial with f_1, f_2 and f_3 as time varying coefficients, the polynomial has only even powers due to the cell symmetry.

$$T(r) = f_1 + f_2\left(r/R\right)^2 + f_3\left(r/R\right)^4 \tag{A.1}$$

By (A.1) the surface temperature is interpreted as $T = f_1 + f_2 + f_3$. By defining (5), the volume averaged temperature and its gradient are obtained by (A.2).

$$\overline{T} = f_1 + f_2/2 + f_3/4 \ , \ \ \overline{\gamma} = 4f_2/3R + 8f_3/5R \tag{A.2}$$

Reverse calculation of coefficients gives:

$$\begin{aligned} &f_1 = 4T - 3\overline{T} - 15R\overline{\gamma}, \ \ f_2 = -18T + 18\overline{T} + 15R\overline{\gamma}/2, \\ &f_3 = 15T - 15\overline{T} - 45R\overline{\gamma}/8 \end{aligned} \tag{A.3}$$

By which (A.1) can be fully calculated. Substituting (A.1) into (3) converts the PDE to a set of ordinary differential equations (ODE) with respect to r as below, which yield the matrix representation of (6).

$$\begin{aligned} &\frac{d\overline{T}}{dt} + \frac{48\beta}{R^2}\overline{T} - \frac{48\beta}{R^2}T + \frac{15\beta}{R}\overline{\gamma} - \frac{\beta}{k_t V_b} = 0 \\ &\frac{d\overline{\gamma}}{dt} + \frac{320\beta}{R^3}\overline{T} - \frac{320\beta}{R^3}T + \frac{120\beta}{R^2}\overline{\gamma} = 0 \end{aligned} \tag{A.4}$$

Considering the boundary conditions of (3) the battery (surface) temperature is obtained as in (6) by (A.5)

$$T = \frac{24k_t}{24k_t + Rh}\overline{T} + \frac{15k_t}{48k_t + 2Rh}\overline{\gamma} + \frac{Rh}{24k_t + Rh}T_\infty \tag{A.5}$$

ACKNOWLEDGMENT

The research was undertaken in collaboration with the WMG Centre High Value Manufacturing Catapult (funded by Innovate UK) in collaboration with Jaguar Land Rover Limited.

REFERENCES

[1] B. Scrosati, J. Garche and W. Tillmetz, Advances in battery technologies for electric vehicles, First Edition,, Oxford: Woodhead Publishing, 2015.

[2] X. Luo, J. Wang, M. Dooner and J. Clarke, "Overview of current development in electrical energy storage technologies and the application potential in power system operation," *Applied energy,* vol. 137, pp. 511-536, 2015.

[3] H. Rahimi-Eichi, U. Ojha, F. Baronti and M. Chow, "Battery management system: An overview of its application in the smart grid and electric vehicles," *IEEE Industrial Electronics Magazine,* vol. 7, no. 2, pp. 4-16, 2013.

[4] F. Sun, R. Xiong and H. He, "Estimation of state-of-charge and state-of-power capability of lithium-ion battery considering varying health conditions," *Journal of Power Sources,* vol. 259, pp. 166-176, 2014.

[5] L. Yang, Y. Cai, Y. Yang and Z. Deng, "Supervisory long-term prediction of state of available power for lithium-ion batteries in electric vehicles," *Applied Energy,* vol. 257, p. 114006, 2020.

[6] A. Farmann and D. Sauer, "A comprehensive review of on-board State-of-Available-Power prediction techniques for lithium-ion batteries in electric vehicles," *Journal of Power Sources,* vol. 329, pp. 123-137, 2016.

[7] D. Kim and D. JUNG, "Method of estimating maximum output of battery for hybrid electric vehicle," US Patent 7,518,375, 2009.

[8] J. Christopherson , "Battery Test Manual for Electric Vehicles," U.S. Department of Energy Vehicle Technologies Program, Revision 3,, Idaho , 2015.

[9] R. Xiong, H. He, F. Sun and K. Zhao, "Online estimation of peak power capability of Li-ion batteries in electric vehicles by a hardware-in-loop approach," *Energies,* vol. 5, no. 5, pp. 1455-1469, 2012.

[10] G. Plett, "High-performance battery-pack power estimation using a dynamic cell model," *IEEE Transactions on vehicular technology,* vol. 53, no. 5, pp. 1586-1593, 2004.

[11] O. Bohlen, "Impedance-based Battery Monitoring," in *PhD dissertation*, Aachen University, 2008.

[12] J. Hu, J. Hu, H. Lin, X. Li, C. Jiang, X. Qiu and W. Li, "State-of-charge estimation for battery management system using optimized support vector machine for regression," *Journal of Power Sources,* vol. 269, pp. 682-693, 2014.

[13] T. Feng, L. Yang, X. Zhao, H. Zhang and J. Qiang, "Online identification of lithium-ion battery parameters based on an improved equivalent-circuit model and its implementation on battery state-of-power prediction," *Journal of Power Sources,* vol. 281, pp. 192-203, 2015.

[14] C. Wei, M. Benosman and T. Kim, "Online parameter identification for state of power prediction of lithium-ion batteries in electric vehicles using extremum seeking," *International Journal of Control, Automation and Systems,* vol. 17, no. 11, pp. 2906-2916, 2019.

[15] C. Burgos-Mellado, M. Orchard, M. Kazerani, R. Cardenas and D. Saez, "Particle-filtering-based estimation of maximum available power state in Lithium-Ion batteries," *Applied Energy,* vol. 161, pp. 349-363, 2016.

[16] T. Kim, W. Qiao and L. Qu, "Online SOC and SOH estimation for multicell lithium-ion batteries based on an adaptive hybrid battery model and sliding-mode observer," in *IEEE Energy Conversion Congress and Exposition*, Denver, CO, 2013.

[17] X. Tang, K. Yao, B. Liu, W. Hu and F. Gao, "Long-term battery voltage, power, and surface temperature prediction using a model-based extreme learning machine," *Energies,* vol. 11, no. 1, p. 86, 2018.

[18] D. Wang, F. Yang, L. Gan and Y. Li, "Fuzzy prediction of power lithium ion battery state of function based on the fuzzy c-means clustering algorithm," *World Electric Vehicle Journal,* vol. 10, no. 1, p. 1, 2019.

[19] E. Chemali, P. Kollmeyer, M. Preindl and A. Emad, "State-of-charge estimation of Li-ion batteries using deep neural networks: A machine learning approach," *Journal of Power Sources,* vol. 400, pp. 242-255, 2018.

[20] R. Xiong, H. He, F. Sun, X. Liu and Z. Liu, "Model-based state of charge and peak power capability joint estimation of lithium-ion battery in plug-in hybrid electric vehicles," *Journal of power sources,* vol. 229, pp. 159-169, 2013.

[21] S. Wang, M. Verbrugge, J. Wang and P. Liu, "Power prediction from a battery state estimator that incorporates diffusion resistance," *Journal of Power Sources,* vol. 214, pp. 399-406, 2012.

[22] W. Waag, S. Käbitz and D. Sauer, "Experimental investigation of the lithium-ion battery impedance characteristic at various conditions and aging states and its influence on the application," *Applied energy,* vol. 102, pp. 885-897, 2013.

[23] W. Waag, C. Fleischer and D. Sauer, "Critical review of the methods for monitoring of lithium-ion batteries in electric and hybrid vehicles," *Journal of Power Sources,* vol. 258, pp. 321-339, 2014.

[24] N. Kim, A. Rousseau and E. Rask, "Parameter estimation for a Lithium-ion battery from chassis dynamometer tests," *IEEE Transactions on Vehicular Technology,* vol. 65, no. 6, pp. 4393-4400, 2016.

[25] F. Quiñones, R. Milocco and S. Real, "Remaining discharge-time prediction for batteries using the Lambert function," *Journal of Power Sources,* vol. 400, pp. 256-263, 2018.

[26] G. Dong, J. Wei, Z. Chen, H. Sun and X. Yu, "Remaining dischargeable time prediction for lithium-ion batteries using unscented Kalman filter," *Journal of Power Sources,* vol. 364, pp. 316-327, 2017.

[27] M. Faraji-Niri, J. Marco, T. Dinh and T. Yu, "Two Layer Markov Model for Prediction of Future Load and End of Discharge Time of Batteries," in *23rd International Conference on Mechatronics Technology IEEE*, Salerno, Italy, 2019.

[28] D. Pola, H. Navarrete, M. Orchard, R. Rabié, M. Cerda, B. Olivares, J. Silva, P. Espinoza and A. Pérez, "Particle-filtering-based discharge time prognosis for lithium-ion batteries with a statistical characterization of use profiles," *IEEE Transactions on Reliability,* vol. 64, no. 2, pp. 710-720, 2015.

[29] C. Pan, W. Dai, L. Chen, L. Chen and . L. Wang, "Driving range estimation for electric vehicles based on driving condition identification and forecast," *AIP Advances,* vol. 7, no. 10, p. 2017, 105206.

[30] C. Sun, F. Sun and H. He, "Investigating adaptive-ECMS with velocity forecast ability for hybrid electric vehicles," *Applied Energy,* vol. 185, pp. 1644-1653, 2017.

[31] G. He, S. Ma and Y. Li, "Study on the short-term forecasting for traffic flow based on wavelet analysis," *System Engineering Theory and Practice,* vol. 9, pp. 101-106, 2002.

[32] L. Ouyang, F. Zhu, G. Xiong, H. Zhao and F. Wang, "Short-term traffic flow forecasting based on wavelet transform and neural network," in *20th International Conference on Intelligent Transportation Systems*, Yokohama, Japan, 2017.

[33] S. Nejad, D. Gladwin and D. Stone, "A systematic review of lumped-parameter equivalent circuit models for real-time estimation of lithium-ion battery states," *Journal of Power Sources,* vol. 316, pp. 183-196, 2016.

[34] Y. Kim, J. Siegel and A. Stefanopoulou, "A computationally efficient thermal model of cylindrical battery cells for the estimation of radially distributed temperatures," in *American Control Conference*, Washington, 2013.

[35] D. Bernardi, E. Pawlikowski and J. Newman, "General energy balance for battery systems," *Journal of the Electrochemical Society,* vol. 132, no. 1, p. 5 – 12, 1985.

[36] . V. R. Subramanian, V. D. Diwakar and D. Tapriyal, "Efficient macromicro macromicro scale coupled modeling of batteries," *Journal of the Electrochemical,* vol. 152, no. 10, pp. 2002-2008, 2005.

[37] Y. Sheng, "Wavelet transform," in *Transform and Applications Handbook,*, Boca Raton, Florida, USA, CRC Press, 2000.

[38] M. Misiti, Y. Misiti, G. Oppenheim and J. e. Poggi.

[39] D. Stroock, An introduction to Markov processes, Springer Science & Business Media, 2013.

[40] L. Li, J. Sun, C. Wang, Y. Zhou and K. Lin, "Enhanced Gaussian process mixture model for short-term electric load forecasting," *Information Sciences,* vol. 477, pp. 386-398, 2019.

[41] A. Dempster, "Maximum likelihood estimation from incomplete data via the EM algorithm," *Journal of the Royal Statistical Society: Series B (Statistical Methodology),* vol. 39, pp. 1-38, 1977.

[42] Y. Cao, X. Wei, H. Dai and Q. Fang, "A Method for Remaining Discharge Energy Prediction of Lithium-Ion Batteries Based on Terminal Voltage Prediction Model," in *IEEE Vehicle Power and Propulsion Conference*, Belfort, France , 2017.

[43] S. Ma, M. Jiang, P. Tao, C. Song, J. Wu, J. Wang, T. Deng and W. Shang, "Temperature effect and thermal impact in lithium-ion batteries: A review," *Progress in Natural Science: Materials International,* vol. 28, no. 6, pp. 653-666, 2018.

[44] M. Jafari, A. Gauchia, K. Zhang and . L. Gauchia, "Simulation and analysis of the effect of real-world driving styles in an EV battery performance and aging," *IEEE Transactions on Transportation Electrification,* vol. 1, no. 4, pp. 391-401, 2015.

[45] M. Faraji Niri, T. Bui, T. Dinh, E. Hosseinzadeh, T. Yu and J. Marco, "Remaining energy estimation for lithium-ion batteries via Gaussian mixture and Markov models for future load prediction," *Journal of Energy Storage,* 2020.

[46] D. Worwood, Q. Kellner, M. Wojtala, W. Widanage, R. McGlen, D. Greenwood and J. Marco, "A new approach to the internal thermal management of cylindrical battery cells for automotive applications," *Journal of Power Sources,* vol. 346, pp. 151-166, 2017.

[47] K. Shah, C. McKee, D. Chalise and A. Jain, "Experimental and numerical investigation of core cooling of Li-ion cells using heat pipes," *Energy,* vol. 113, pp. 852-860, 2016.

[48] A. Loges, S. Herberger, P. Seegert and T. Wetzel, "A study on specific heat capacities of Li-ion cell components and their influence on thermal management," *Journal of Power Sources,* vol. 336, pp. 341-350, 2016.

[49] E. Shireman, D. Steinley and M. Brusco, "Examining the effect of initialization strategies on the performance of Gaussian mixture modeling," *Behavior research methods ,* vol. 49, no. 1, pp. 282-293, 2017.

[50] Q. Kellner, E. Hosseinzadeh, G. Chouchelamane , W. Widanage and J. Marco, "Battery cycle life test development for high-performance electric vehicle applications," *ournal of Energy Storage,* vol. 15, pp. 228-244, 2018.

Mona Faraji Niri received her Ph.D. degree in Control engineering from Iran University of Science and Technology, Tehran, Iran, in 2016. She is currently a research fellow at Warwick Manufacturing Group, The University of Warwick, United Kingdom. Her research interests include, electric vehicle control, battery modelling, battery management systems, stochastic, robust control algorithms and machine learning.

Truong Q. Dinh is currently Assistant Professor in Energy Management and System Control. He completed the first-class Ph.D. mechatronics degree in the School of Mechanical Engineering at University of Ulsan, South Korea in the early of 2010. His research interests mainly concentrate on Machine design and optimization, system engineering and power management and control, renewable energy and advanced propulsion system design and control.

James Marco is a professor at Warwick University, a chartered engineer and fellow of the institutions of engineering and technology (IET). His research interests include system engineering, real time control and systems modelling. In recent years this has focused on the application of these generic techniques to underpin new battery system designs, model and control algorithms.

Tung F. Yu is an engineer at Jaguar Land Rover Ltd, he has been involved in EV development since 2017. He received his Ph.D. in Physics in 2013 and MEng in Electronic Engineering in 2009 from the University of Warwick, United Kingdom. His main interest is transferring scientific and engineering research in the area of batteries and electric vehicles into real life applications.

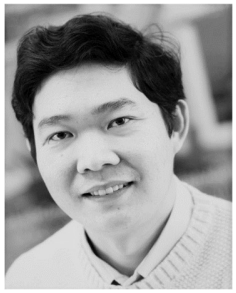

Truong M.N. Bui pursued his doctoral research in Mechatronics at the School of Mechanical Engineering, University of Ulsan, S. Korea. He joined Warwick Manufacturing Group, The University of Warwick, United Kingdom as. He is highly interested in control theory and applications: nonlinear, adaptive, and robust control, fault tolerant control for hybrid mechatronics systems, energy storage, management and verification for EV/HEVs applications.